Agricultural Water Management 333 (2026) 110643

Contents lists available at ScienceDirect

Agricultural Water Management

journal homepage: www.elsevier.com/locate/agwat

Unraveling drought impacts on winter wheat yield in the Yellow River Basin: A coupled drought index–crop modeling framework

Yingnan Wei [a,b], Zhijian He [a], Ning Yao [b,c,*], Ben Niu [b], Genghong Wu [a], Xiaotao Hu [b], La Zhuo [a], Hao Feng [a], Qiang Yu [a]

[a] State Key Laboratory of Soil and Water Conservation and Desertification Control, College of Soil and Water Conservation Science and Engineering, Northwest A&F University, Yangling, Shaanxi 712100, China
[b] College of Water Resources and Architectural Engineering, Key Lab of Agricultural Water and Soil Engineering of Education Ministry, Northwest Agriculture and Forestry University, Yangling, Shaanxi 712100, China
[c] Institute of Arid Meteorology, CMA/ Key laboratory of Arid Climatic Change and Reducing Disaster of Gansu Province, Key Open Laboratory of Arid Climatic Change and Disaster Reduction of CMA, China

ARTICLE INFO

Keywords:
Non-stationary drought index
Crop model
Winter wheat
Yield reduction
Yellow River Basin

ABSTRACT

As a core region for winter wheat production in China, the Yellow River Basin (YRB) is increasingly exposed to drought stress, posing a substantial threat to national food security. Quantifying drought-induced yield losses and unraveling their underlying mechanisms are therefore essential for developing adaptive management strategies. This study integrated meteorological, soil, historical drought, winter wheat growth and yield data to construct a coupled analytical framework. The non-stationary Standardized Precipitation Evapotranspiration Index (NSPEI) and the Standardized Soil Moisture Index (SSI) were employed jointly with an improved DSSAT-CERES-Wheat model to investigate the spatiotemporal characteristics of drought across the YRB from 1961 to 2021, and to assess its impacts on winter wheat development and yield reduction from 1981 to 2021. The results underscored a declining trend in both NSPEI and SSI values within the Yellow River Basin over the study period, signifying an intensification of drought conditions. Notably, agricultural drought exhibited a discernible lagged response relative to meteorological drought. During the winter wheat growing seasons from 1981 to 2021, the nine-month timescale drought indices showed a certain consistency with the water stress factor (WFTD) simulated by the improved DSSAT model in some drought years, indicating that crop water stress intensified as drought conditions became more severe. Deep-layer soil moisture (10–40 cm and 40–100 cm) deficit emerged as an important determinant of severe winter wheat yield reduction in the YRB, conveying a markedly higher level of yield loss certainty than meteorological or shallow-soil droughts, which afford only limited buffering capacity under mild water stress. This study advances the mechanistic understanding of drought-yield relationships by integrating non-stationary climate indices with biophysical crop modeling. Our framework provides actionable insights for drought monitoring, risk assessment, and mitigation strategies in semi-arid agricultural systems.

1. Introduction

Climate warming has intensified the global drought trend, leading to increased drought-affected areas, longer durations, and higher frequencies (Dai, 2011; Duncan et al., 2015). Since the late 1970s, the frequency of droughts has been increasing, threatening national food security and social stability (AghaKouchak et al., 2014; Wang et al., 2023a; Yang et al., 2024). In recent years, the frequency, duration, and intensity of droughts have risen in the Yellow River Basin, posing a growing threat to food production (Li et al., 2024). There are four types of drought: meteorological, agricultural, hydrological, and socio-economic, each corresponding to deficiencies in precipitation, soil moisture, runoff, and water for socio-economic development, respectively (Dracup et al., 1980). Agricultural drought is defined by a decline in soil moisture that reduces crop yields or leads to crop failure, even in the absence of surface water resources (Mishra and Singh, 2010). To better assess the impact of drought on crop growth, various drought indices have been developed, such as the Palmer Drought Severity Index

* Correspondence author at: College of Water Resources and Architectural Engineering/Key Lab of Agricultural Water and Soil Engineering of Education Ministry, Northwest Agriculture and Forestry University, Yangling, Shaanxi 712100, China.
E-mail address: yaoning@nwafu.edu.cn (N. Yao).

https://doi.org/10.1016/j.agwat.2026.110643
Received 7 May 2026; Received in revised form 12 July 2026; Accepted 13 July 2026
Available online 17 July 2026
0378-3774/

(PDSI) (Palmer, 1965), Standardized Precipitation Index (SPI) (McKee et al., 1993), Standardized Precipitation Evapotranspiration Index (SPEI) (Vicente-Serrano et al., 2010), Standardized Soil Moisture Index (SSI) (Martinez-Fernandez et al., 2016; Mpelasoka et al., 2008; Sadri et al., 2018; Trnka et al., 2015). Among these, the SPEI comprehensively considers the influence of precipitation, temperature fluctuations, and solar radiation on regional drought, and it was widely used in the analysis of regional drought distribution and the monitoring of agricultural droughts (Li et al., 2021; Ng et al., 2024; Potop et al., 2012; Yao et al., 2020a). The SSI accounts for the influence of soil moisture on agricultural drought and has been widely used as an index for evaluating and predicting agricultural drought across various soil types (Kumar and Chu, 2024; Shyrokaya et al., 2024).

Studies on the spatiotemporal dynamics of drought patterns in the Yellow River Basin have made significant progress globally. The SSI-based assessment of agricultural drought indicates an increase in drought events, although their rate of occurrence has slowed (Li et al., 2024). Over half of the regions experience drought recovery periods lasting more than four months (Liu and Xue, 2022), with notable spatial variability in drought vulnerability (Wu et al., 2013). Analysis of historical wet-dry changes using various drought indices shows a widespread trend toward desertification in most areas, with the northwest facing more severe drought conditions (Wang et al., 2024; Zhao et al., 2021). The propagation of meteorological drought into hydrological drought has been influenced by human activities, which have amplified regional differences and slowed the rate of propagation (Wang et al., 2023c). Additionally, multi-scale SPEI in the basin shows a positive correlation with the global "OCO-2" solar-induced chlorophyll fluorescence (SIF) data, with average SIF values during the growing season displaying a distinct spatial pattern of higher values in the south and lower values in the north (Geng et al., 2022). Although previous studies have used various drought indices to monitor the characteristics of droughts in the Yellow River Basin, most of these studies are based on stationary drought indices. This approach has its limitations and may overestimate the impact of climate change on future droughts (Wen et al., 2020). Therefore, research that integrates non-stationary meteorological drought indices, which account for meteorological variability, and agricultural drought indices that consider soil moisture, to deeply explore the spatiotemporal evolution of droughts in the Yellow River Basin, remains relatively limited.

Currently, there are several methods for assessing the impact of drought on winter wheat growth, including field water control experiments (Li et al., 2010a; Zhang et al., 2017), crop growth models (Bai et al., 2024; Rahimi-Moghaddam et al., 2021), and statistical analyses (Javed et al., 2021; Shi et al., 2024). Some studies have investigated how water availability at different growth stages affects winter wheat development and yield, identifying the greening and grain-filling stages as critical for field water management (Yao et al., 2015c). Other research has combined meteorological and agricultural drought indices with the DSSAT-CERES-Wheat model, emphasizing a stronger connection between agricultural drought and wheat growth in the Loess Plateau region (Chen et al., 2020). However, research that combines field experiments with the CERES-Wheat model aims to elucidate the response mechanisms of winter wheat to water stress and has indicated that the CERES-Wheat model has certain limitations in simulating winter wheat growth under complex drought conditions (Yao et al., 2020b). At that time, most studies were limited by experimental conditions, model accuracy, and analysis methods. Although the response mechanism of winter wheat yield to drought had been clarified, the results had certain limitations. Therefore, in order to reduce the uncertainty of a single method, it was necessary to combine multiple methods to analyze the impact of drought on winter wheat growth (Sun et al., 2021).

To address these gaps, this study integrates both meteorological and soil moisture data from the Yellow River Basin to analyze the spatiotemporal evolution of drought using the Non-Stationary Standardized Precipitation Evapotranspiration Index (NSPEI) and the SSI. By combining these indices with historical drought events and field experiments, we aim to assess the ability of these indices to monitor drought with greater accuracy and sensitivity. By revealing spatiotemporal patterns of drought across different growth stages of winter wheat, this research allows for a more precise quantitative assessment of drought's impact on crop yield and provides predictions for yields under various drought scenarios. Ultimately, the findings contribute to better drought prevention, mitigation, and food security strategies in the Yellow River Basin.

2. Materials and methods

2.1. Study area and data source

The Yellow River is the second longest river in northern China, running from west to east across nine Chinese provinces, and finally merging into the Bohai Sea in Shandong. The basin ranges from 95°53' to 119°05' E, 32°10' to 41°50' N, with a total area of 7.95×10^5 km^2. To better analyze the spatial heterogeneity of winter wheat growth and drought response, the basin was divided into three regions according to the agricultural regionalization of China, together with differences in topography, climatic conditions, soil moisture regimes, and winter wheat site distribution. Region 1 corresponds to the arid and semi-arid agricultural region of northern China, where precipitation is relatively limited and crop growth is strongly affected by water availability. Region 2 represents the Qinghai–Tibet Plateau agricultural region, which is characterized by high elevation, low temperature, and distinct hydrothermal conditions. Region 3 includes the Loess Plateau and Huang–Huai–Hai Plain agricultural regions, where winter wheat is more widely distributed and irrigation plays an important role in crop production. These regions show clear differences in elevation, precipitation, temperature, soil water conditions, and cropping systems, which may lead to different responses of winter wheat to meteorological and agricultural drought. Therefore, this regional division provides a reasonable basis for investigating spatial differences in winter wheat drought response and yield reduction risk across the Yellow River Basin (Fig. 1).

The daily meteorological data for the Yellow River Basin from 1961 to 2021 were obtained from the China Meteorological Data Service Center (http://data.cma.cn/). The dataset includes daily records of precipitation, relative humidity, temperature, wind speed, and sunshine duration. Additionally, phenological data collected from observation stations between 1992 and 2013, as well as winter wheat yield data recorded from 2000 to 2013, were also sourced from the same data center and used for the calibration and validation of the crop model. The winter wheat phenology data included the anthesis date and maturity date. Based on the parameter adjustment and validation requirements of the DSSAT-CERES-Wheat model, 14 winter wheat stations with complete data for three years or more were selected.

Soil data, including soil moisture and physical parameters, were obtained through the Google Earth Engine (GEE) platform (https://code.earthengine.google.com/). For stations with both meteorological data and winter wheat phenological observations, this study extracted daily soil moisture data at depths of 0–10 cm, 10–40 cm, 40–100 cm, and 100–200 cm from the GLDAS dataset for the period 1961–2021. Data on soil physical parameters, including bulk density, field capacity, and wilting coefficient, were sourced from the Cold and Arid Regions Science Data Center National Earth Science Data Platform (http://westdc.westgis.ac.cn/). The types, sources, and sampling details of all datasets can be found in Wei et al. (2025).

2.2. Computation of drought indices

The study had selected both meteorological and agricultural drought indices to analyze drought conditions in the Yellow River Basin. However, the commonly used meteorological drought indices, such as the

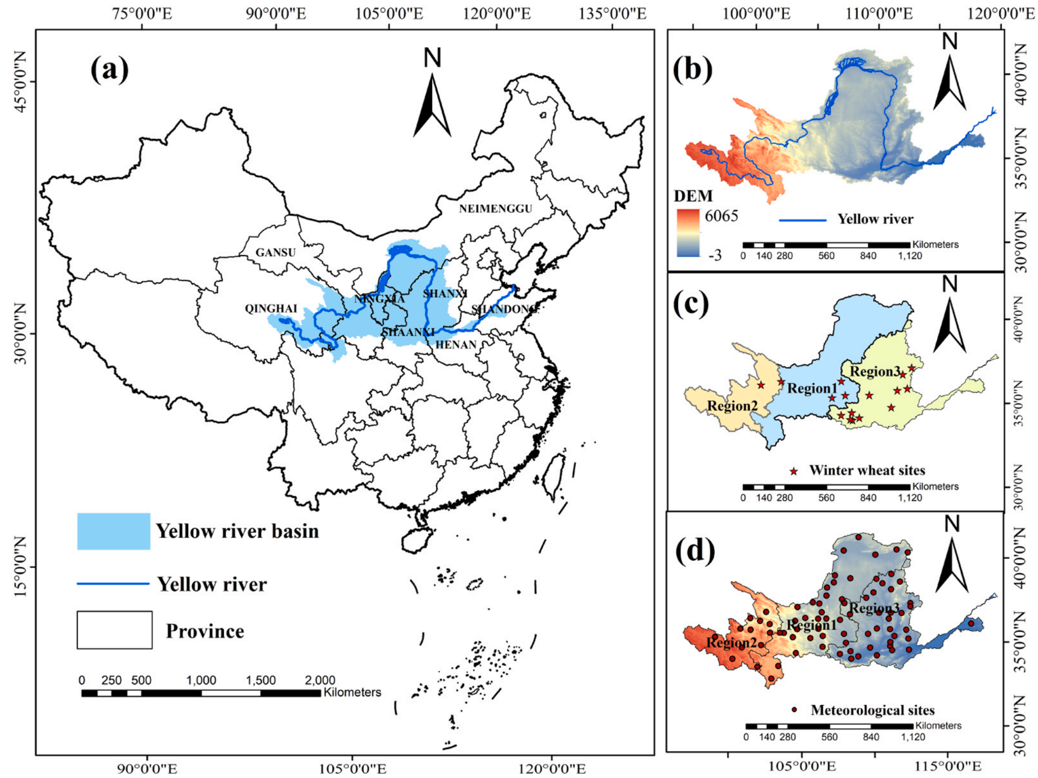

Fig. 1. Information of the Yellow River Basin. (a) Geographical location, (b)Elevation, (c) Study area division and winter wheat site, (d) Meteorological site.

SPEI, were typically based on stationary models. In these models, the location parameter (γ) of the probability density function fitted to the dataset using a three-parameter log-logistic distribution was fixed and did not change dynamically with the characteristics of different datasets. This stationary approach did not account for non-stationarity in the data, which meant that the resulting meteorological drought indices might not accurately reflect the true severity of drought. To address this issue, the study employed the NSPEI and the SSI for drought assessment and monitoring in the Yellow River Basin. These indices were better suited to capture the trends in meteorological and soil variables, thereby increasing the accuracy of drought assessments and more closely aligning with historical drought events.

The NSPEI is an optimized version of the traditional SPEI. The SPEI had defined the difference between precipitation and potential evapotranspiration as the water deficit (D) and fitted this deficit using a probability function with a stationary three-parameter log-logistic distribution, which included scale, shape, and location parameters. The fitted probability distribution was then standardized to compute the SPEI. However, in traditional SPEI calculations, the fitting function for the water deficit was fixed, and the location parameter was constant, which introduced some inaccuracies. In contrast, the NSPEI based on the GAMLSS framework incorporates non-stationarity by allowing the distribution parameters, especially the location and scale parameters, to vary with time, leading to a more reasonable and accurate assessment of meteorological drought in the Yellow River Basin (Wen et al., 2020). In this study, R language and the Generalized Additive Models for Location, Scale, and Shape (GAMLSS) framework were used, together with the Akaike Information Criterion (AIC) and Schwarz Bayesian Criterion (SBC), to select the most appropriate probability distribution function for the water deficit D from several candidate distributions and to construct the optimal GAMLSS model. By allowing the distribution parameters, especially the location parameter μ and scale parameter σ, to vary over time in stationary, linear, or nonlinear forms, the model can better capture the non-stationary characteristics of the water deficit series. This approach improves the accuracy of meteorological drought assessment using the NSPEI. First, the FAO56 Penman-Monteith equation (Allen et al., 1998) was used to estimate monthly reference evapotranspiration (ET_0). The cumulative D over different timescales was calculated as follows:

$$D = P - ET_0 \tag{1}$$

where P is the monthly precipitation (mm).

The optimal probability distribution function was selected from several candidate distributions using the GAMLSS framework, with model performance evaluated by AIC and SBC. This fitting process determined the time-varying sequences of the location parameter μ and scale parameter σ. (Niu et al., 2024). Taking the gamma distribution as an example, the cumulative probability $F(x)$ can be calculated by integrating the fitted probability density function:

$$F(x) = \int_0^x f(x|\mu,\sigma)dx \tag{2}$$

.

Finally, the series was standardized to a normal distribution to obtain the NSPEI. The specific calculation was as follows:

$$NSPEI = w - \frac{c_0 + c_1 w + c_2 w^2}{1 + d_1 w + d_2 w^2 + d_3 w^3} \tag{3}$$

$$w = \sqrt{-2\ln P(x)} \tag{4}$$

where $c_0 = 2.515517$, $c_1 = 0.802853$, $c_2 = 0.010328$, $d_1 = 1.432788$, $d_2 = 0.189269$, $d_3 = 0.001308$ (Vicente-Serrano et al., 2010). If $P(x) \leq 0.5$, then $P(x) = 1–F(x)$. If $P(x) > 0.5$, $P(x)$ is replaced by $1 - P(x)$, and the NSPEI value is assigned the opposite sign.

The Standardized Soil Moisture Index (SSI) was first developed by Hao, AghaKouchak, (2013) and was calculated in a manner similar to the SPI. However, unlike precipitation data, soil moisture content typically does not follow a unimodal distribution; instead, it often displays bimodal, multimodal, or skewed distributions (Vidal et al., 2010).

Therefore, using the Kernel Density Estimation (KDE) method, a non-parametric test approach, provided a better fit for these types of distributions. In the KDE method, the kernel function (K) and bandwidth (h) of the probability density function significantly affected the fitting accuracy. The choice of kernel function had a relatively minor effect, while the bandwidth selection had a more substantial impact. If the bandwidth was too large or too small, it could result in underfitting or overfitting, respectively (Rajagopalan et al., 1997; Silverman, 1986; Weng et al., 2015). In this study, the KDE method was used to fit the soil moisture data from various stations in the Yellow River Basin. KDE allowed for the fitting of multimodal distributions of soil moisture data. The bandwidth of the probability density function was dynamically optimized based on changes in soil moisture content. After calculating the cumulative kernel density function, it was standardized to obtain the SSI. The specific calculation process was as follows:

For each site's time series, the probability density function (PDF) of soil moisture content was given by:

$$f(x) = \frac{1}{Nh}\sum_{i=1}^{N} K\left(\frac{x - x_i}{h}\right) \tag{5}$$

where N represents the total number of years; x_i is the soil moisture content in the current period for the i-th year; $K(x)$ is the kernel function; h is the bandwidth. Here, the Gaussian kernel function, which fits the majority of soil moisture variation patterns, is chosen as the kernel function:

$$K(x) = \frac{1}{\sqrt{2\pi}}e^{-\frac{x^2}{2}} \tag{6}$$

.

The bandwidth was calculated using a rule of thumb, which defaulted to the minimum of 0.9 times the standard deviation and the interquartile range divided by the sample size raised to the power of $-1/5$, consistent with Silverman's "rule of thumb" (Silverman, 1986). This calculation was performed using the “density” function in R, which estimated the probability density function. Integrating the probability density function yielded the cumulative probability function. By standardizing this cumulative probability function, the Standardized Soil Moisture Index (SSI) was obtained.

$$F(x) = \int_{-\infty}^{x} f(u)du \tag{7}$$

.

To evaluate the spatiotemporal evolution of drought conditions in the Yellow River Basin, this study analyzed drought indices at 1, 3, 6, and 12-month timescales. These timescales corresponded to changes in moisture conditions on a monthly, seasonal, semi-annual, and annual basis. Additionally, the moisture conditions during the 9-month winter wheat growing season (from sowing in October of the previous year to harvest in June of the current year) significantly affected the growth and development of winter wheat. Therefore, calculating the NSPEI and SSI drought indices during the winter wheat growing season was essential to accurately assess the impact of drought on crop development. Normal, mild, moderate, severe, and extreme drought conditions correspond to NSPEI or SSI intervals of $(-0.5, 0.5]$, $(-1.0, -0.5]$, $(-1.5, -1.0]$, $(-2.0, -1.5]$ and ≤ -2.0, respectively.

2.3. Analysis of the spatiotemporal evolution of drought

2.3.1. Mann-Kendall trend analysis

The trend analysis utilized the Modified Non-parametric Mann-Kendall (MMK) method, which considered all significant autocorrelations within the time series. This method did not require the sample to follow a specific distribution and effectively reduced interference from a few outliers. Hamed and Rao (1998) improved the accuracy of trend tests by accounting for lag-i autocorrelation (usually $i = 1$), which could significantly affect the results, thereby eliminating the autocorrelated component from the time series. The MMK test was used to detect trends in meteorological variables, such as precipitation (P), maximum temperature ($T_{\max}$), minimum temperature ($T_{\min}$), relative humidity (RH), wind speed (W_s), and sunshine duration (n), as well as drought indices, including NSPEI and SSI, in the Yellow River Basin during the historical period from 1961 to 2021.

When the test statistic Z* is greater than zero, it indicates an increasing trend in the time series; when Z* is less than zero, it indicates a decreasing trend. Under the null hypothesis of no trend, the standardized MMK test statistic approximately follows a standard normal distribution. Therefore, ± 1.96 was used as the critical value for a two-tailed significance test at the 95% confidence level ($p < 0.05$). Specifically, $Z^* > 1.96$ indicates a significant increasing trend, whereas $Z^* < -1.96$ indicates a significant decreasing trend (Li et al., 2010b). The MMK test statistic Z* is calculated as follows:

$$Z* = \frac{Z}{\sqrt{n/n*}} \tag{8}$$

where n is the total number of data points and n^* may be the length of the sequence after adjusting for autocorrelation.

The Sen's slope was calculated for meteorological variables (such as P, T_{max}, T_{min}, RH, W_s, n) and drought indices (NSPEI and SSI) in the Yellow River Basin during the historical period (1961–2021). Sen (1968) calculated the trend slope using Kendall’s Tau rank correlation coefficient method, known as Sen’s slope. The calculation is given as below:

$$b = Median\left(\frac{x_j - x_i}{j - i}\right) i < j \tag{9}$$

where x_i and x_j are the data points in the time series, and i and j are their corresponding time indices.

2.3.2. Wavelet analysis

Wavelet analysis was a method that used a set of wavelet functions to represent a signal. It was used to separate the periodicities of drought indices on seasonal and interannual timescales. By transforming the time series signal into the time-frequency domain, the primary patterns of variation could be identified, along with how these patterns changed over time. The mother wavelet function was expressed by the following equation (Torrence and Compo, 1998):

$$\int_{-\infty}^{+\infty} \psi(t)dt = 0 \tag{10}$$

where t represents time; $\psi(t)$ is the wavelet function, which can be translated and scaled along the time axis to form a family of functions.

$$\psi_{a,b}(t) = |a|^{-1/2}\psi\left(\frac{t-b}{a}\right), a, b \in R, a \neq 0 \tag{11}$$

where $\psi_{a,b}$ (t) is the wavelet; a reflects the wavelet length factor; b is the time translation factor. Morlet wavelet is used as the basis function and MATLAB is used for wavelet analysis.

2.3.3. Run theory

In order to identify and quantify drought events, this study utilized Run theory to calculate the duration, intensity, and frequency of drought events (Wu et al., 2017; Wu and Chen, 2019). This method could provide a more intuitive understanding of the temporal and spatial distribution of drought in the Yellow River basin.

The Run theory used different thresholds to identify drought events (Fig. 2 and Table S1). Drought scenarios are divided into two types. In the first scenario, when the threshold falls below lower thresholds (R_l), a drought event is recorded, with a drought intensity of S_0 and a duration of D_0. In the second scenario, there is a minor wet event of short duration

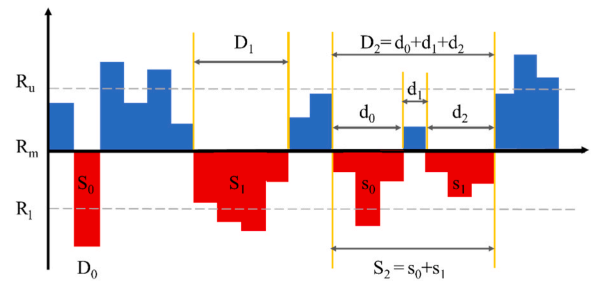

Fig. 2. Schematic diagram of each variable in run theory. The symbols in the figure are described in the main text. R_u, R_m, and R_l represent the upper, middle, and lower thresholds for drought events under each drought category, respectively, and are used to distinguish different drought scenarios within each drought category. D_0, D_1, and D_2 denote drought duration, while S_0, S_1, and S_2 denote drought intensity.

between two drought events, with the wet duration being less than six months and the threshold below upper threshold (R_u). In this case, the two drought events are treated as a single drought event. This is depicted in Fig. 2 as d_0, d_1, and d_2. Here, the total drought duration is $D_2 = d_0 + d_1 + d_2$, and the drought intensity is $S_2 = s_0 + s_1$.

Based on Run theory and the 12-month time scale NSPEI, the years 1961–2021 were divided into 1961–1970, 1971–1980, 1981–1990, 1991–2000, 2001–2010, and 2011–2021. This classification was used to analyze the temporal and spatial variability of drought in the Yellow River Basin, focusing on the intensity, duration, and frequency of drought events. The spatial distribution characteristics of extreme drought, severe drought, and moderate drought in the Yellow River Basin were identified by the Run theory. The study did not separate out mild drought because it had little impact on crop growth and development. Therefore, mild drought was combined with normal conditions (which were applied throughout the study).

2.4. CERES-Wheat model

The DSSAT model, developed by the United States Department of Agriculture, was a sophisticated crop model. The CERES-Wheat model, integrated into the Cropping System Model (CSM) platform (DSSAT v4.7), simulated soil carbon, nitrogen, and water balance, as well as the growth, development, and yield of wheat. By inputting meteorological, soil, crop management, and crop parameter data into the model, it could simulate various growth factors such as phenology and yield from sowing to harvest (Jones et al., 2003). The DSSAT-CERES-Wheat model typically operated on a daily scale, simulating processes including canopy solar radiation absorption and photosynthesis, root nutrient uptake, assimilation and allocation, water uptake and transpiration, growth and respiration, leaf area expansion, organ growth and senescence, and field management (Dar et al., 2021; Ding et al., 2021; Gunawat et al., 2022; Liu et al., 2019; Zhang et al., 2019).

Identifying a reasonable set of genetic parameters was key to enhancing model prediction accuracy (Wei et al., 2022; Yao et al., 2022). The DSSAT-CERES-Wheat model included seven genetic parameters (Table 1). The model parameters were estimated using the GLUE method with 10,000 iterations to obtain a set of reasonable genetic parameters for winter wheat. In this study, winter wheat yield from 1981 to 2021 was simulated using the CERES-Wheat model. The period 1961–1980 was not included in the yield simulation because reliable winter wheat phenological and yield observation data were unavailable, which could not support model calibration and validation. During the 1981–2021 simulation period, crop management practices were kept consistent across years to highlight the effects of drought on winter wheat yield. Specifically, all simulations were conducted under rainfed conditions. Due to the lack of long-term and spatially consistent crop management records across the study area, temporal changes in fertilization and tillage practices were not explicitly considered in this study.

Table 1
Definitions and ranges of genetic parameters of winter wheat in the DSSAT-CERES-Wheat model.

Parameters	Parameters definition	Parameters range	Unit
P1V	The number of days required to pass the vernalization stage at the optimum temperature	5–65	d
P1D	Photoperiod parameter	0–95	%
P5	Accumulated temperature in grain filling period	300–800	℃ d
G1	Number of seeds per crown mass at anthesis period	15–30	No g^{-1}
G2	Standard grain weight under optimal conditions	20–65	mg
G3	Standard dry weight per stem and ear at maturity without stress	1–2	g
PHINT	The accumulated temperature needed to complete the growth of a leaf	60–100	℃ d

This study used an improved DSSAT-CERES-Wheat model to simulate winter wheat growth in the Yellow River Basin from 1981 to 2021. The data used for model calibration and validation were randomly divided at a ratio of 70% and 30%, with 70% used for model calibration and the remaining 30% used for model validation. Model performance was evaluated using the relative mean absolute error (RMAE) and relative root mean square error (RRMSE) (He et al., 2010). The improved DSSAT-CERES-Wheat model used a nonlinear SWFAC to quantify the effect of drought stress on winter wheat yield. Compared with the original model, the RMAE of the improved model decreased by 13.7%, indicating that the overall simulation accuracy of the model was improved (Yao et al., 2025).

2.5. Assessment of yield reduction

Under rainfed conditions, drought could lead to reduced yields of winter wheat. This study used the yield reduction rate to reflect the extent of yield loss caused by drought to winter wheat.

$$y = (Y_r - Y)/Y_r \times 100\% \tag{12}$$

where y is the yield reduction rate, %; Y is the winter wheat yield in drought years, kg/ha; Y_r is the reference yield in the absence of drought, kg/ha. In this study, the trend yield was used as the reference yield under non-drought conditions. It mainly reflects long-term yield changes caused by non-climatic factors, such as technological progress, cultivar improvement, and advances in management practices, and was estimated from the 1981–2021 winter wheat yield series using the quadratic exponential smoothing method. The difference between Y and Y_r was considered to be mainly driven by climatic variability and was therefore used to characterize drought-related yield loss (Boken, 2000; Duan and Niu, 2018; Liu et al., 2025).

To quantitatively analyze the impact of drought on winter wheat yield, this study first performed a normality test on yield anomalies under different drought intensities and soil depths. Based on the standardized drought indices (NSPEI and SSI at different soil layers), three drought categories were defined: mild, moderate, and severe-or-above drought. Because the number of extreme drought samples was limited, severe and extreme droughts were combined into a single severe-or-above drought category to ensure the robustness of the statistical analysis. Combined with Quantile-Quantile plots (Q-Q Plot) and normal fitting histograms, a visual diagnosis of the data distribution characteristics for each subgroup was conducted (Fig. S1). In addition, the Shapiro-Wilk test was used for quantitative statistical verification. The results showed that the p-values of all subgroups were greater than 0.05, indicating that there was no significant evidence against the normality assumption for yield anomalies under different drought scenarios.

On the basis of verifying the normality hypothesis, the conditional probability distribution of yield under different drought grades was further calculated. For multi-source drought indices (NSPEI and SSI $_{0–10\ cm}$, SSI $_{10–40\ cm}$, and SSI $_{40–100\ cm}$), the cumulative distribution functions (CDF) of yield anomalies were respectively fitted. Through the conditional probability model $P\ (Y \leq y \mid D)$, the probability response of the target yield reduction level (y) under a specific drought intensity (D) was quantitatively evaluated. By comparing the horizontal displacement laws of the CDF curves under different drought gradients, the sensitivity differences of winter wheat yield in the Yellow River Basin in response to

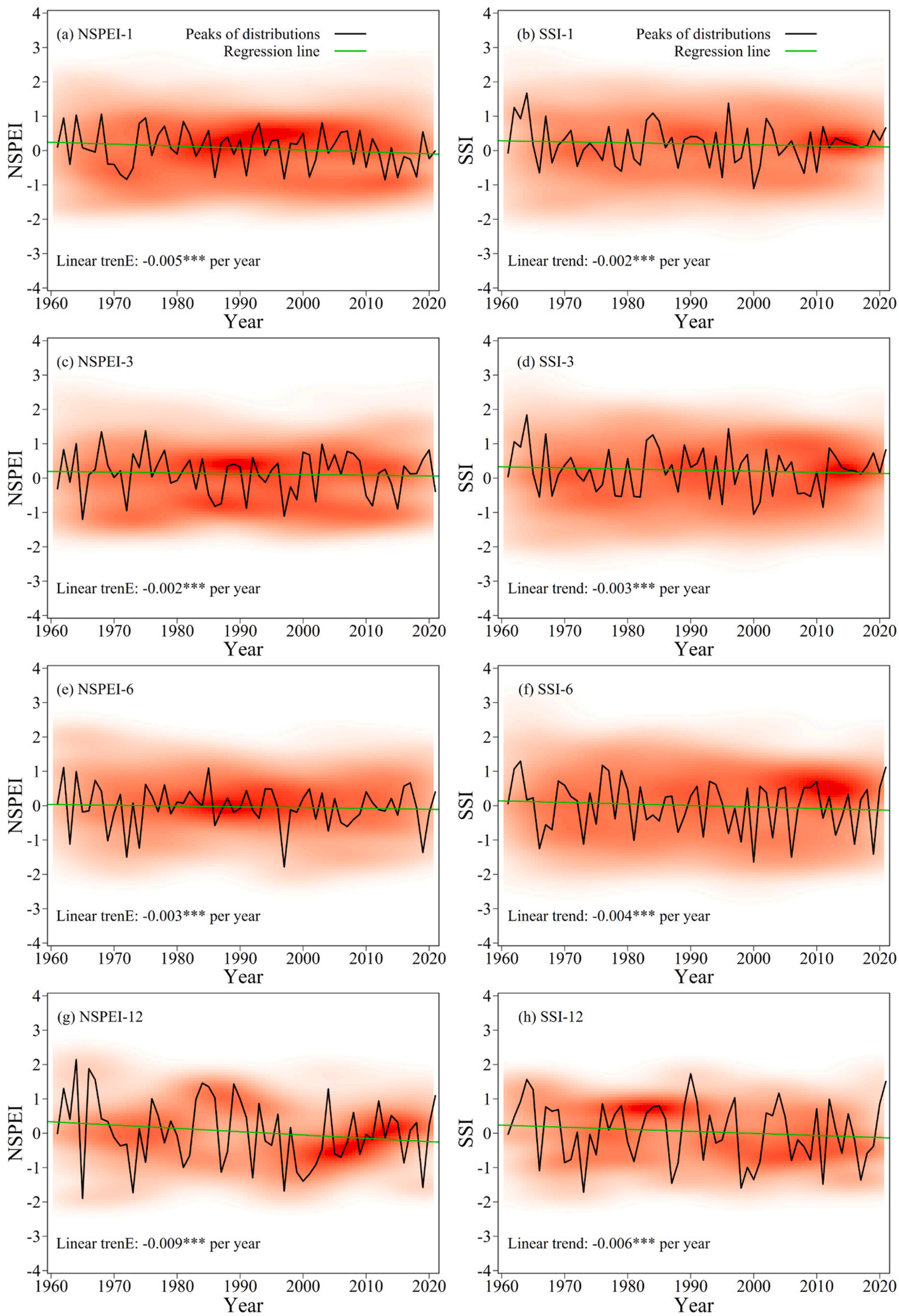

Fig. 3. Temporal variation trend of non-stationary standardized precipitation Evapotranspiration Index (NSPEI) and standardized soil moisture Index (SSI $_{0–10\ cm}$) at different time scales in the Yellow River Basin from 1961 to 2021. The red shaded areas represent the density distribution of NSPEI or SSI. The black solid line indicates the maximum NSPEI or SSI distribution density. The green solid line shows the linear slope. The symbols '*, **, and ***' represent $p < 0.05$, $p < 0.01$, and $p < 0.001$ significance levels, respectively.

drought propagation in different soil layers were profoundly revealed. Meanwhile, Pearson correlation analysis was used to verify the relationship between drought intensity and yield loss.

3. Results

3.1. Temporal variation of different drought indices

The NSPEI values of various time scales were mainly concentrated in the range of −1.5–1.5 over 1961–2021 (Fig. 3). The linear slopes of NSPEI for the 1, 3, 6, and 12-month timescales were −0.005, −0.002, −0.003, and −0.009, respectively. This demonstrated that NSPEI decreased with the increase of time after considering the non-stationarity of meteorological factors, indicating a significant drought trend in the Yellow River Basin during 1961–2021 ($p < 0.001$). The negative troughs of NSPEI were less pronounced at the 1- and 3-month timescales, suggesting that severe drought was not evident on these two scales. In contrast, the 6-month and 12-month timescales showed larger NSPEI peaks with more pronounced fluctuations. At the 6-month timescale, NSPEI values were notably low in 1974 and 1997, reflecting the occurrence of severe droughts. At the 12-month timescale, the NSPEI values in years such as 1965, 1974, 1997, and 2019 fell below −1.5, indicating more severe drought conditions.

The linear slopes of the SSI for the 0–10 cm soil layer at the 1, 3, 6, and 12-month timescales were −0.002, −0.003, −0.004, and −0.006, respectively (Fig. 3). For the 10–40 cm soil layer, the linear slopes were −0.004, −0.006, −0.005, and −0.012, respectively (Fig. S2). In the 40–100 cm soil layer, the slopes were −0.005, −0.009, −0.011, and −0.014, respectively (Fig. S3). The results indicated that, according to the agricultural drought index, the trend of dryness and wetness changes in the Yellow River Basin from 1961 to 2021 was consistent with the meteorological drought index results, showing a trend toward increasing drought. Compared to the SSI at monthly timescales, the SSI at annual timescales showed a more gradual change. The SSI peaks for the 0–10 cm soil layer were higher than those for the 10–40 cm and 40–100 cm soil layers, indicating that the surface soil was wetter, while deeper soil layers contained lower moisture and were more prone to drought. Notably, years such as 1966, 1974, 1988, and 1998 experienced more intense agricultural drought, with SSI values falling below −1.0.

Based on the temporal variation graphs of NSPEI and SSI at different timescales, it was evident that the slopes were negative, indicating that drought conditions in the Yellow River Basin intensified from 1961 to 2021. Meteorological drought tended to precede agricultural drought, suggesting a certain lag effect in the onset of agricultural drought. Additionally, the slope values for agricultural drought were larger than those for meteorological drought, implying that the trend towards drought was more pronounced in agricultural drought compared to

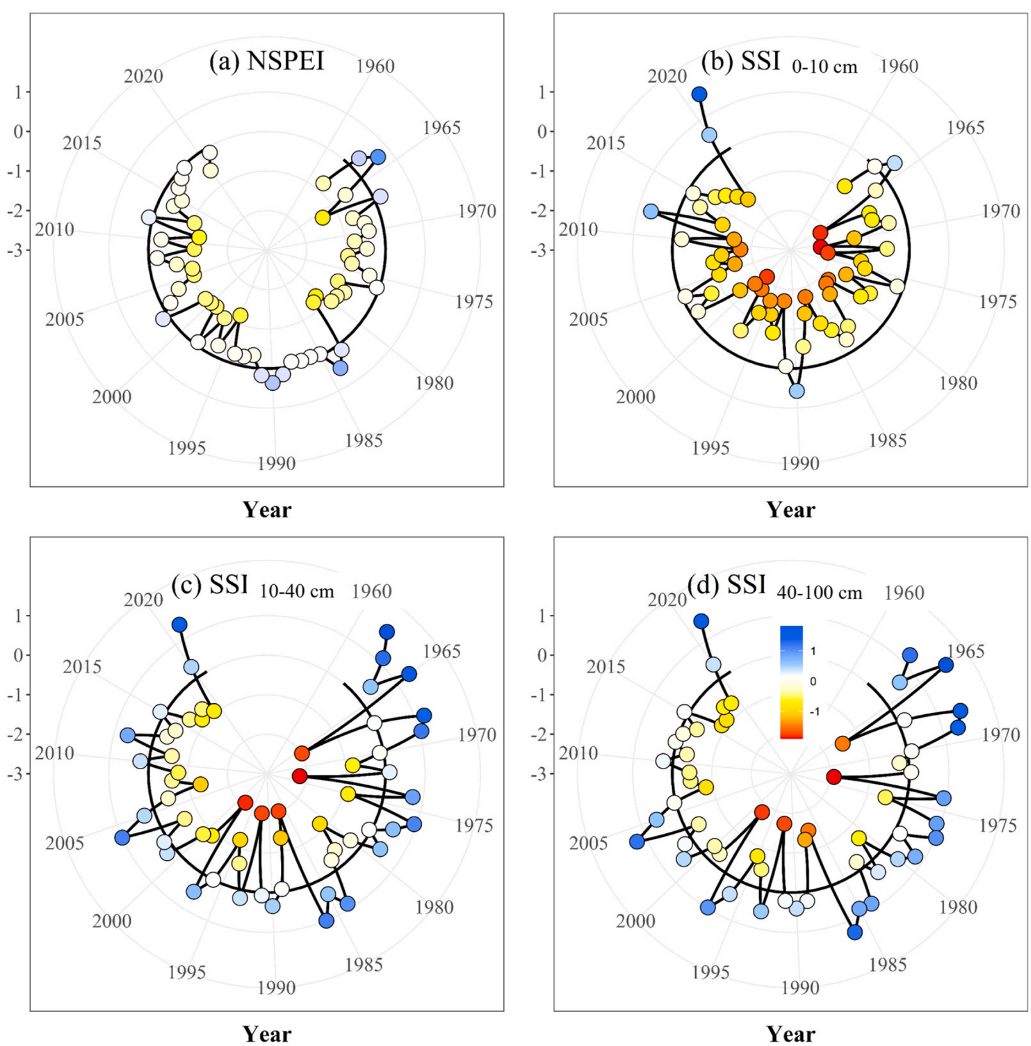

Fig. 4. Temporal variation of drought index during winter wheat growth period in the Yellow River Basin from 1961 to 2021. The black semicircle line indicates a drought index of 0. The dots of different colors represent the drought index, with red indicating drought and blue indicating wet. The darker the color means the higher the value, the more severe the drought or wet degree.

meteorological drought.

Drought conditions, indicated by NSPEI and SSI, were prevalent during the winter wheat growing season, particularly for NSPEI and the SSI $_{0–10\ cm}$ (Fig. 4). Over the 61 years from 1961 to 2021, years with a drought index greater than 0 were rare: only 10 years for NSPEI and just 6 years for the SSI $_{0–10\ cm}$ soil layer. Most years during the winter wheat growing season experienced drought conditions. While the SSI for the 10–40 cm and 40–100 cm soil layers showed more wet years over the 61-year period, drought still occurred in the majority of years. From 1961–2021, the probability of drought clearly increased over time. However, there were no years with NSPEI values below −1.5, indicating that severe drought did not occur. The SSI of the 0–10 cm soil layer was around −1.0 in most years, indicating frequent moderate drought. Severe drought conditions, where the SSI approached −2.0, were observed in 1966, 1971, 1973, and 1999. The SSI for the 10–40 cm soil layer typically indicated mild drought, with moderate and severe droughts being rare; significant drought occurred only in 1973, 1987, 1992, and 1998. The SSI for the 40–100 cm soil layer showed similar results to the 10–40 cm layer, but severe drought was even less frequent, occurring mainly in 1973, 1992, and 1998. Overall, agricultural drought appeared to be more severe than meteorological drought. The SSI for the 0–10 cm soil layer indicated the most severe drought, followed by the 10–40 cm and 40–100 cm layers. Some years experienced severe droughts. While NSPEI indicated drought in many years, the drought severity was relatively low, mostly classified as mild, which had a limited impact on the growth and development of winter wheat.

The trends and drought identification patterns of NSPEI and SSI were generally consistent. To evaluate the ability of the drought indices to identify actual drought events, representative stations from three different regions of the Yellow River Basin were selected in this study. The drought processes identified by the 12-scale NSPEI and SSI at different soil layers during 1961–2021 were compared with historical drought records (Fig. S4). The results showed that NSPEI could effectively capture the timing of historical drought events. Overall, NSPEI can reliably identify historical drought events, while SSI provides complementary information on the severity of agricultural drought across different soil layers (Fig. S4).

3.2. Spatiotemporal distribution of drought characteristics

The spatial distribution of different drought indices across the basin was generally consistent, with slight differences in significance (as shown in Fig. 5 and Table S2). Over the past 61 years, the Sen's slope of non-stationary meteorological and agricultural drought indices in most areas of the Yellow River Basin was negative, indicating a drying trend. In contrast, positive values were observed in the western part of the basin, with minimal changes in the far eastern region, suggesting that the eastern part maintained the most stable moisture conditions. There were slight variations between the changes in NSPEI and the SSI at different soil depths (0–10 cm, 10–40 cm, 40–100 cm). NSPEI showed positive values in both the southern and northern parts of the basin, while the SSI at all three soil depths exhibited positive values only in the northern part, with Sen's slope values smaller than those of NSPEI. The range of Sen's slope values was smallest for NSPEI and SSI $_{10–40\ cm}$, indicating the most significant variability in moisture conditions. SSI $_{0–10\ cm}$ had the largest positive Sen's slope (sen slope = 0.0040), while SSI $_{40–100\ cm}$ had the smallest negative Sen's slope (sen slope = −0.0032). As shown in Table S2, out of the 77 stations across the Yellow River Basin, more than 40 stations exhibited a decreasing trend, most of which were statistically significant. A small number of stations showed an increasing trend, but the changes were not significant. Overall, from 1961 to 2021, there was some spatial variability in NSPEI and SSI across the Yellow River Basin, but the overall trend indicated an intensification of drought conditions.

From 1961–2021, the intensity of drought in the Yellow River Basin gradually increased (Fig. S5). Between 2011 and 2021, there were stations where the intensity of moderate, severe, and extreme droughts all ranged from 41% to 50%. Severe drought, in particular, had a higher number of stations with drought intensity exceeding 30% compared to moderate and extreme droughts. Most stations with drought intensity greater than 40% were concentrated in the midstream region of the Yellow River Basin, indicating that the midstream region experienced higher drought intensity. Moderate drought reached its peak intensity from 2001 to 2010, with two stations recording drought intensity of 50%. Most cases of extreme drought had intensities between 0% and 10%, but these increased over time, with many stations showing drought intensities between 30% and 50% by the 2011–2021 period.

The overall duration of drought in the Yellow River Basin increased from 1961 to 2021, with the longest durations occurring during 2001–2011 (Fig. 6). The average duration of all drought types across the Yellow River Basin was approximately seven months. Extreme and moderate droughts each had durations of around three months, with the longest durations observed from 2011 to 2021. Severe droughts lasted about four months, with the longest durations occurring during the periods 1981–1990 and 2001–2010, reaching around five months. The longer duration of severe drought compared to moderate and extreme

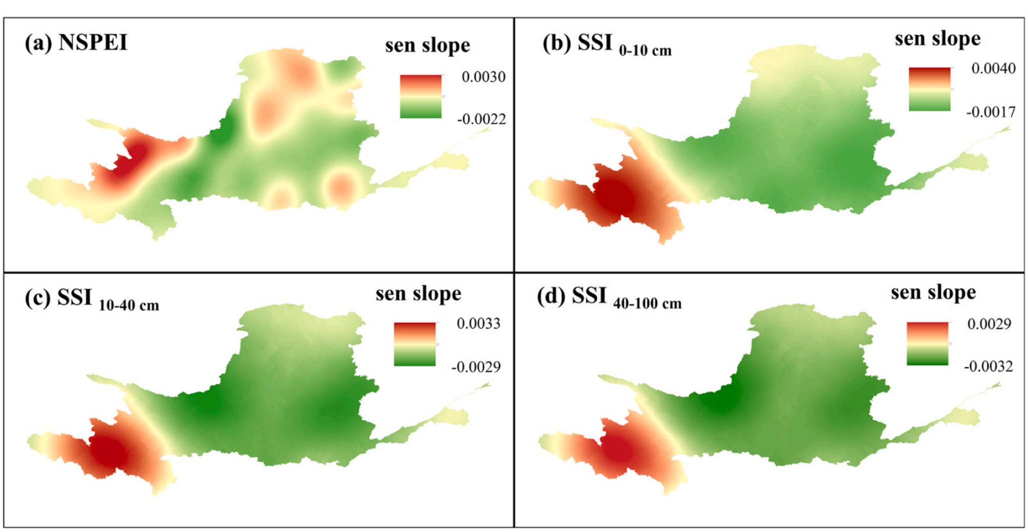

Fig. 5. Spatial distribution of Sen's slope of drought index on 12-month time scale in the Yellow River Basin from 1961 to 2021. (a)-(d) indicates NSPEI, SSI $_{0–10\ cm}$ soil layer, SSI $_{10–40\ cm}$ soil layer and SSI $_{40–100\ cm}$ soil layer during the growth period of winter wheat, respectively.

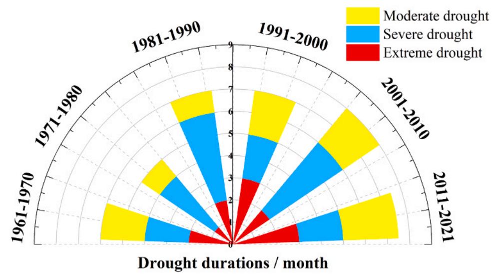

Fig. 6. Different drought durations in the Yellow River Basin from 1961 to 2021. Different sectors indicate different time periods, including 1961–1970, 1971–1980, 1981–1990, 1991–2000, 2001–2010, and 2011–2021. The colors represent drought categories: yellow indicates moderate drought, blue indicates severe drought, and red indicates extreme drought.

droughts indicates that the drought conditions in the Yellow River Basin were particularly severe from 1961 to 2021.

This study divided the period from 1961 to 2021 into decadal intervals and analyzed the frequency of three types of drought: extreme, severe, and moderate (Fig. 7). The results indicated that extreme droughts occurred less frequently than moderate and severe droughts. Among the different drought levels, moderate droughts were the most frequent, with an average frequency ranging from 3 to 5 occurrences, showing an overall increasing trend, reaching 5 occurrences in the period from 2011 to 2021. Severe droughts followed, with an average frequency of 1–3 occurrences. Extreme droughts were the least frequent overall, generally averaging 0–1 occurrence in most periods. However, their frequency increased from 1961 to 2010 and peaked at nearly 3 occurrences during 2001–2010, before decreasing to 1 occurrence during 2011–2021. Severe droughts were most frequent during 1991–2000, with an average frequency of approximately 3 occurrences.

The drought index at the 12-month time scale exhibited the strongest periodicity (Fig. S6). In contrast, the 1-month time scale SSI for the 0–10 cm soil layer, the 3-month time scale NSPEI, and the 0–10 cm soil layer SSI showed no significant periodicity. The SSI for the 10–40 cm and 40–100 cm soil layers exhibited similar periodic oscillations, with a cycle of 4–7 years observed for the SSI from 1983 to 1992. The periodic signal was more pronounced in the SSI for the 10–40 cm soil layer.

3.3. Quantitative evaluation of winter wheat yield losses under drought

The specific genetic parameters of winter wheat phenology and yield simulation in three regions of the Yellow River Basin by using the

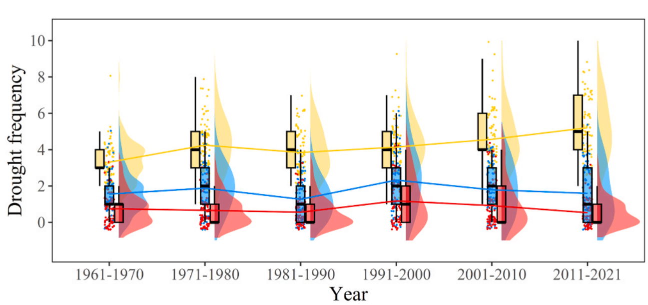

Fig. 7. Cloud and rain map of different drought frequency in the Yellow River Basin from 1961 to 2021. Yellow represents moderate drought, blue represents severe drought, and red represents extreme drought. The solid black lines in each box chart represent the median frequency of the time period, the upper and lower boundaries of the box chart represent the upper and lower quartiles of the frequency, and the whisker lines above and below the box chart represent the 90th and 10th percentiles of the frequency, respectively. The half-violin diagram shows the frequency density. Scatter points represent different frequencies. The broken line is the average line from 1961 to 2021, showing the changing trend of the frequency of different types of drought.

improved DSSAT-CERES-Wheat model were shown in Table S3. The improved DSSAT-CERES-Wheat model demonstrated high reliability in simulating winter wheat phenology and yield (Table S4). For phenological dates, RMAE and RRMSE values remained below 10%, with the maturation date showing higher precision (RMAE: 1.46–4.02%) than anthesis. Although yield simulation errors were relatively higher, all RMAE and RRMSE values remained within a robust range of 6.31–18.41%. Notably, Region 1 exhibited superior simulation accuracy compared to Regions 2 and 3. Overall, with all error metrics for both calibration and validation under 20%, the model proved well-suited for simulating winter wheat growth dynamics in the Yellow River Basin. Therefore, using the improved DSSAT-CERES-Wheat model to simulate winter wheat growth and yield formation in the Yellow River Basin was feasible.

Using the calibrated DSSAT-CERES-Wheat model, simulations were conducted for all winter wheat sites in the three regions of the Yellow River Basin, covering anthesis date (ADAP), maturity date (MDAP), yield (HWAM), aboveground biomass (CWAM), maximum leaf area index (LAI), and evapotranspiration (ET) (Fig. 8). Both ADAP and MDAP showed decreasing trends from 1981 to 2021, indicating that the anthesis and maturity dates of winter wheat occurred earlier over time. Region 2 had the latest anthesis and maturity dates, whereas Region 3 had the earliest, likely due to differences in geographic location and altitude. HWAM and CWAM both showed a decreasing trend, with region 2 having higher yield and biomass compared to regions 1 and 3. LAI fluctuated between 1 and 9, showing a decreasing trend in region 2. The ET fluctuated around 1.0 from 1981 to 2021, but showed an upward trend, with higher ET in regions 1 and 3 compared to region 2.

WFTD showed a certain consistency with NSPEI and SSI in some drought years (Fig. S7). In Region 1, the representative site was Huanxian in Gansu Province, where WFTD fluctuated between approximately 0 and 0.6, showing large interannual variability. In Region 2, the representative site was Minhe in Qinghai Province, where WFTD ranged from about 0.4–0.7, with smaller fluctuations than those in Regions 1 and 3. In Region 3, the representative site was Linfen in Shanxi Province, where WFTD fluctuated between approximately 0 and 0.6. Overall, WFTD was slightly higher and more stable in Region 2, indicating relatively weaker crop water stress in this region. In years with lower NSPEI and SSI values, WFTD also decreased in most cases, suggesting that meteorological drought and soil moisture drought could partly explain crop water stress. However, this relationship varied among sites, indicating that WFTD was also influenced by crop growth stage, soil water supply, root water uptake, and local environmental conditions.

Winter wheat yield reduction rates in the Yellow River Basin exhibit significant spatiotemporal heterogeneity (Fig. 9). In Region 1, yield losses were slightly higher before 2000 than after 2000, but the overall magnitude of yield reduction was relatively small, with a maximum value of 35%. Yield reduction events in Region 2 were more episodic, but some years experienced substantial losses, reaching up to 57%. These severe losses were mainly concentrated between 1990 and 2000 and were mostly associated with soil drought indicated by SSI $_{10–40\ \mathrm{cm}}$, and SSI $_{40–100\ \mathrm{cm}}$. In contrast, Region 3 showed more continuous drought-related yield losses after 2000, but the overall intensity was lower than that in Region 2. The consistency between severe yield reduction (>30%) and SSI in deep soil layers indicates that water deficits in the 10–40 cm and 40–100 cm soil layers had a more pronounced effect on winter wheat yield loss than short-term meteorological drought. Overall, deep layer soil moisture conditions are an important factor influencing severe yield reduction events.

The conditional CDF of winter wheat yield in the Yellow River Basin showed different responses to meteorological and soil droughts (Fig. 10). Overall, as drought intensity increased from mild to severe or extreme levels, the CDF curves shifted leftward, indicating an increased probability of negative yield anomalies under stronger drought conditions. The response magnitude differed among drought indices, with soil drought indices generally showing stronger relationships with yield

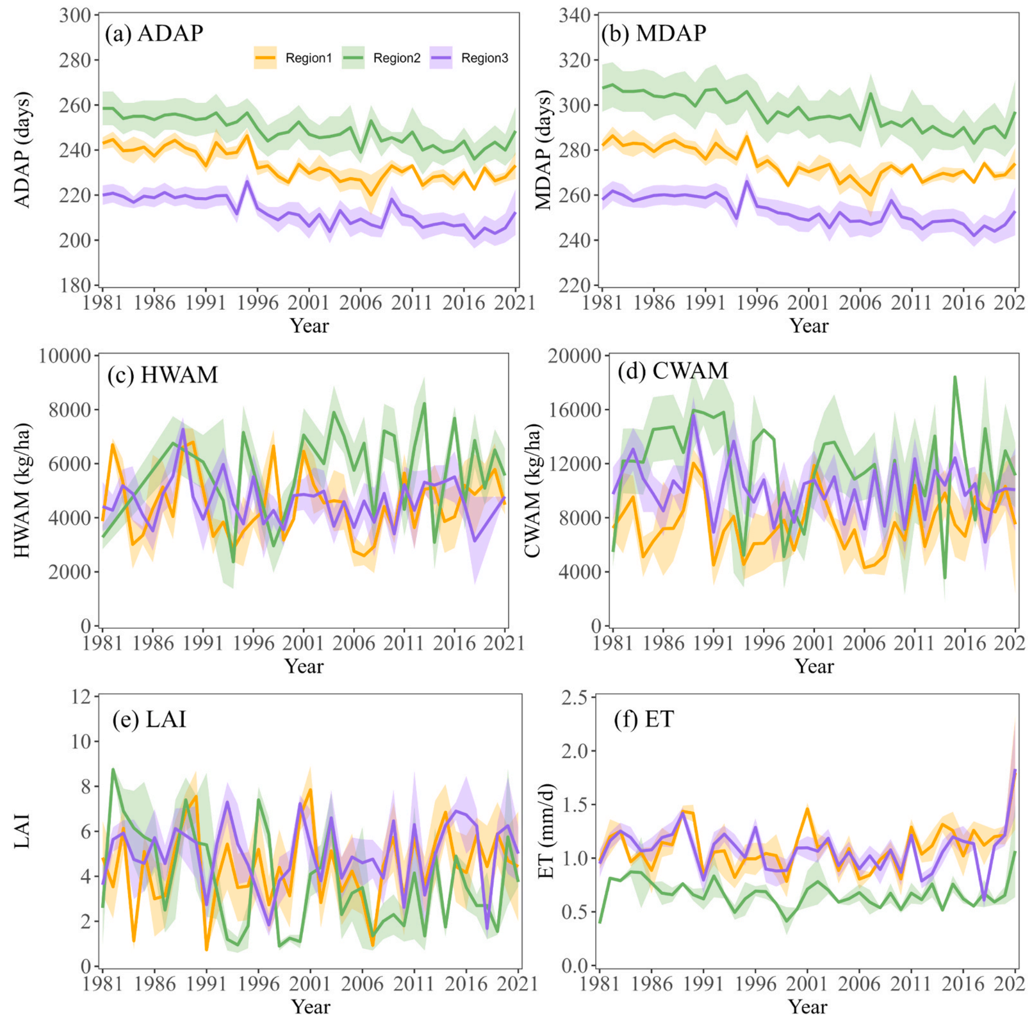

Fig. 8. Changes of (a) anthesis (ADAP), (b) maturity (MDAP), (c) yield (HWAM), (d) aboveground biomass (CWAM), (e) leaf area index (LAI) and (f) transpiration (ET) of winter wheat in the Yellow River Basin during historical periods. Yellow represents region 1, green represents region 2, purple represents region 3. The shaded areas indicate the standard deviation bands.

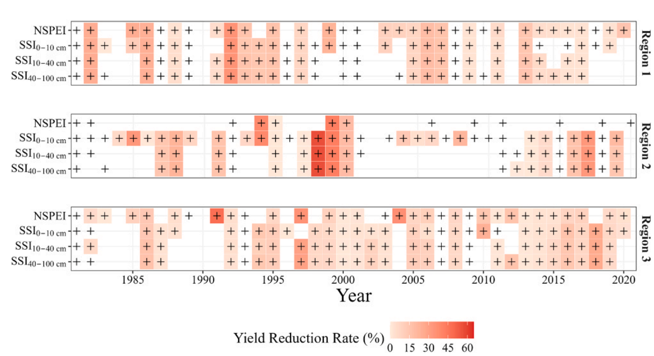

Fig. 9. Yield reduction rates of winter wheat under drought stress across three regions of the Yellow River Basin from 1981 to 2021. " + " denotes the occurrence of drought. Shading indicates the yield reduction rate, with darker colors denoting greater yield losses.

anomalies than the meteorological drought index. In particular, SSI $_{10–40\ cm}$ and SSI $_{40–100\ cm}$ showed the strongest correlations with yield anomalies ($|r| > 0.34$), whereas NSPEI and SSI $_{0–10\ cm}$ exhibited relatively weaker correlations. Comparisons among soil layers further indicated that water deficits in the middle and deep soil layers had a more pronounced effect on winter wheat yield loss. Under SSI $_{10–40\ cm}$ and SSI $_{40–100\ cm}$ conditions, stronger drought categories corresponded to higher conditional probabilities near Yield Anomaly = 0 (Table S5), suggesting that intensified middle- and deep-layer soil drought increased the likelihood of negative yield anomalies. In contrast, the curves for NSPEI and SSI $_{0–10\ cm}$ showed relatively smaller separation among drought categories, indicating that short-term meteorological drought and shallow soil moisture variation had more limited explanatory power for yield loss. Overall, at Yield Anomaly = 0, the conditional probability of negative yield anomalies under stronger drought conditions was generally close to or greater than 50%, with higher probabilities associated with middle- and deep-layer soil drought. This suggests that soil moisture conditions in the 10–40 cm and 40–100 cm layers are important factors influencing winter wheat yield loss risk in the Yellow River Basin (Table S5).

4. Discussion

4.1. Suitability of drought indices

Previous studies have suggested that, compared with stationary drought indices, non-stationary drought indices can provide more accurate assessments of the spatiotemporal variations and propagation characteristics of drought (Niu et al., 2024). NSPEI has also been reported to outperform the traditional stationary SPI in capturing drought

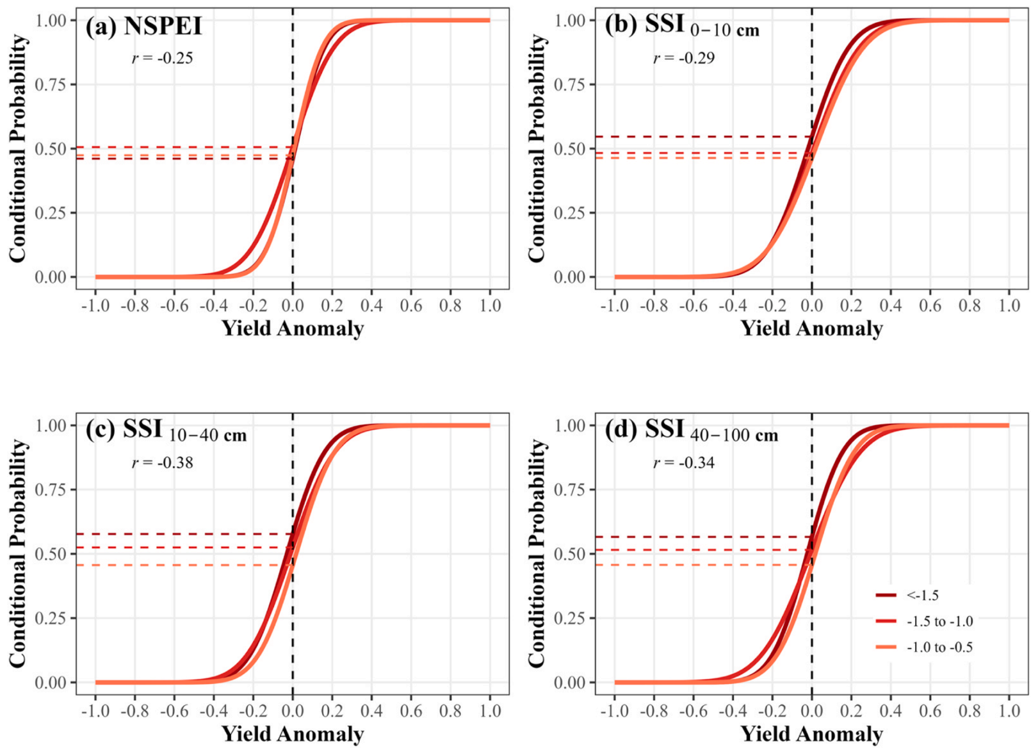

Fig. 10. Conditional probability of winter wheat yield anomaly relative to the values of (a) NSPEI, (b) SSI $_{0\text{–}10\ cm}$, (c) SSI $_{10\text{–}40\ cm}$, and (d) SSI $_{40\text{–}100\ cm}$ in the Yellow River Basin. The values of *r* indicate Pearson correlation coefficients between drought indices and winter wheat yield reduction rate.

characteristics under non-stationary climatic conditions (Chiru Naik et al., 2023; Rashid and Beecham, 2019). The Generalized Additive Model for Location, Scale, and Shape (GAMLSS), which incorporates time-varying location parameters, was used to fit non-stationary drought index distributions, and it was found that non-stationary drought indices provided more accurate estimates of drought characteristics under climate change scenarios (Dixit and Jayakumar, 2022). In particular, the Non-Stationary Standardized Runoff Index (NSRI) was used to assess the impacts of climate change and human activities on hydrological drought, confirming the non-stationarity of hydrological processes in the basin (Wang et al., 2023b). Based on the non-parametric KDE method, SSI obtained by selecting the optimal bandwidth according to soil moisture characteristics, was found to have a stronger ability to describe drought conditions (Ji, 2022). This study utilized the NSPEI developed based on the GAMLSS model and the SSI calculated using the KDE method to diagnose drought in the Yellow River Basin from 1961 to 2021, demonstrating their effectiveness in capturing the spatiotemporal dynamics of drought with higher accuracy compared to traditional methods (Fig. 6).

4.2. Drought evolution in the Yellow River Basin

Research on the spatiotemporal changes of drought in the Yellow River Basin garnered widespread attention. Three typical spatiotemporal distribution patterns of interannual drought in the Yellow River Basin were identified: the whole basin type, the southeast-to-northwest type, and the east-to-west type (Zhou et al., 2021). Studies found a decreasing trend in the SPEI across the Yellow River Basin, with a smaller decrease in the downstream regions of the eastern part of the basin (Wang et al., 2023c). Analysis using various drought indices revealed that most areas within the basin had become progressively drier from 1950 to 2016 (Wang et al., 2022). The risk of drought occurrence was found to vary across different regions of the Yellow River Basin, with the midstream region facing a higher risk compared to other areas (Huang et al., 2015), and agricultural drought was found to be more concentrated in the western part of the basin (Niu et al., 2024). The results of this study indicated that both the NSPEI and the SSI were decreasing over time, leading to increasing aridity in the basin. Specifically, the midstream region was experiencing a more severe trend towards dryness, while the downstream region showed smaller changes in the slope of aridity, with slower drought development. These findings were consistent with previous research.

4.3. Evaluation of winter wheat yield due to drought

Climate change and human activities impact winter wheat growth, leading to extensive research by scholars (Han et al., 2023; Wu et al., 2022). Climate change has been shown to impact the growth and yield of winter wheat (Tao et al., 2022). For instance, rising temperatures have led to the advancement of phenological stages and a subsequent decline in yield (Xu et al., 2020), with the anthesis and maturity stages advancing by an average of 0.19 and 0.1 days per year, respectively (Liu et al., 2018). In the Guanzhong plain, higher average temperatures have shortened the vegetative and reproductive phases of winter wheat, consequently affecting yield (Wu et al., 2022). Our study found that amidst global warming, both the anthesis and maturity dates of winter wheat in the Yellow River Basin have advanced from 1981 to 2021, along with a trend of decreasing yield. However, there are differences among the three regions; compared to regions 1 and 3, region 2 exhibits longer phenological stages and higher yields, which is consistent with previous research.

This study further elucidates the underlying mechanism of how multi-dimensional water deficits impact crop yields. The results indicate that the conditional CDF curves of winter wheat yield exhibit a distinct leftward shift as drought intensity escalates (Fig. 10), quantitatively confirming the non-linear response relationship between drought severity and yield reduction risk (Leng and Hall, 2019). To further verify the explanatory role of deep soil moisture deficits in yield losses, we supplemented the probability analysis of winter wheat yield reduction under different drought conditions (Table S5). The results showed that the probability of yield reduction generally increased with drought severity. Under severe drought conditions (< -1.5), the probabilities were 0.46, 0.55, 0.57, and 0.57 for NSPEI, SSI $_{0–10\ cm}$, SSI $_{10–40\ cm}$, and SSI $_{40–100\ cm}$, respectively. This indicates that deep-layer soil drought was more consistent with winter wheat yield reduction events than meteorological drought and surface soil drought, particularly under severe drought conditions (Fig. 9; Table S5). This suggests that in the Yellow River Basin, deep-layer soil moisture is the key determinant for winter wheat's resilience against sustained drought. This can be attributed to the filtering and lag effects during the evolution of drought from the atmosphere to the soil, which allow deep-layer soil moisture dynamics to more accurately capture the substantial impacts of agricultural drought. When meteorological drought occurs, winter wheat can still compensate for and buffer water stress by utilizing deep-layer soil water storage through its well-developed root system (Li et al., 2026). However, depletion of deep-soil water reserves eliminates the crop's final buffer, leading to irreversible and inevitable yield losses.

Numerous studies had employed crop models to simulate the growth, phenology, and yield of winter wheat (Ishaque et al., 2023; Long et al., 2022). The overall root mean square error (RMSE) for yield simulation using the DSSAT model had been 13%, yet there was significant uncertainty associated with individual model simulations (Kassie et al., 2016). Parameter uncertainty in the MANIHOT model had been found to significantly impact predictions, with uncertainties being 2–5 times higher under high-temperature conditions compared to low-temperature conditions (Moreno-Cadena et al., 2020). An analysis using three DSSAT wheat models had revealed that the uncertainty in yield simulation was greater than that for phenology, with higher uncertainties in regions experiencing high temperatures and drought (Liu and Xue, 2022). In this study, we had utilized an improved DSSAT-CERES-Wheat model to simulate the growth and yield of winter wheat in the Yellow River Basin, observing that the accuracy of yield simulation was lower than that for phenological stages. The uncertainty in yield simulation had been attributed to factors such as planting density, management practices, and sowing dates, which could lead to simulation errors.

4.4. Limitations and future outlook

Despite the insights into the impacts of drought on winter wheat in the Yellow River Basin, several limitations remain. Regarding field management practices, due to the lack of long-term and spatially consistent crop management records across the study area, the DSSAT model simplified the spatial heterogeneity and long-term changes in management practices such as irrigation, fertilization, and tillage. This simplification may introduce uncertainty into yield simulations, because farmers' management decisions and adaptive practices may create microclimatic buffering effects that existing modeling frameworks cannot fully capture. Therefore, the simplification of crop management practices should be regarded as one of the limitations of this study. Future research could further optimize these model inputs by integrating high-resolution satellite-derived management maps, agricultural statistics, or social survey data. This study focused on revealing the impacts of drought on winter wheat from the perspectives of meteorological and agricultural drought, yet has not fully explored the interactions among multiple environmental stressors. Particularly under future climate scenarios, the synergistic effects of heat stress and CO_2 fertilization may alter the sensitivity of winter wheat to deep-soil water deficits. Subsequent research should incorporate these factors to more comprehensively assess crop resilience. On a broad geographical scale, the calibration of genetic parameters for winter wheat still faces severe challenges. Future research should prioritize strengthening the deep application of multi-source data assimilation technologies (such as Sun-Induced Fluorescence, SIF, and remote sensing-based soil moisture) within crop modeling frameworks. By using data assimilation schemes to bridge the scale gap between micro-plot physiological mechanisms and macro-regional yield estimation, it will not only significantly improve the accuracy of drought early-warning systems but also provide solid scientific support for the adaptive allocation and precision scheduling of agricultural water resources in water-scarce basins.

5. Conclusions

The NSPEI and SSI exhibited a significant negative trend in the Yellow River Basin from 1961 to 2021, indicating a trend towards increasing drought. Spatial heterogeneity was observed, with some areas in the western part of the basin showing a wetting tendency. During the winter wheat growing season, SSI exhibited more variability, while NSPEI showed relatively smoother changes. The 12-month drought indices showed the strongest periodicity. NSPEI performed well in identifying historical drought events, while SSI provided complementary information on agricultural drought severity across different soil layers.

Drought intensified with increasing severity in the Yellow River Basin over the past 61 years. Since 2000, sites with drought intensity exceeding 40% emerged, particularly in the midstream region. Drought duration initially decreased but then increased, fluctuating between 3 and 4 months. The frequency and duration of moderate droughts had increased overall over the past 61 years, reaching up to 5 occurrences and 4 months during 2011–2021.

The simulation results from the improved DSSAT-CERES-Wheat model were relatively stable. Region 2 had higher yields and above-ground biomass compared to other areas, with lower ET from 1981 to 2021. During the winter wheat growing season, WFTD showed a certain consistency with NSPEI and SSI in some drought years. Deep-layer soil moisture is an important determinant of severe winter wheat yield reductions in the Yellow River Basin, exerting a more persistent and severe impact than meteorological or shallow-soil droughts.

CRediT authorship contribution statement

Qiang Yu: Writing – review & editing, Methodology. **Genghong Wu:** Writing – review & editing. **Xiaotao Hu:** Methodology. **La Zhuo:** Writing – review & editing, Funding acquisition. **Hao Feng:** Resources. **Yingnan Wei:** Writing – review & editing, Writing – original draft, Data curation. **Zhijian He:** Data curation. **Ning Yao:** Writing – review & editing, Writing – original draft, Funding acquisition, Formal analysis. **Ben Niu:** Methodology.

Declaration of Competing Interest

The authors declare that they have no known competing financial interests or personal relationships that could have appeared to influence the work reported in this paper.

Acknowledgments

This research was financially supported by the National Natural Science Foundations of China (U2243235 and 52209070), Arid Meteorology Science Research Fund (IAM202305), and Cyrus Tang Foundation Project. We thank Tehseen Javed for the linguistic assistance during the preparation of this manuscript.

Appendix A. Supporting information

Supplementary data associated with this article can be found in the online version at doi:10.1016/j.agwat.2026.110643.

Data availability

Data will be made available on request.

References

AghaKouchak, A., Cheng, L., Mazdiyasni, O., Farahmand, A., 2014. Global warming and changes in risk of concurrent climate extremes: insights from the 2014 California drought. Geophys. Res. Lett. 41 (24), 8847–8852.

Allen, R., Pereira, L., Raes, D., Smith, M., 1998. Crop Evapotranspiration-Guidelines for Computing Crop Water Requirements. In: FAO Irrigation and Drainage Paper, 56. FAO, Rome, Italy.

Bai, H.Z., Xiao, D.P., Tang, J.Z., Liu, D.L., 2024. Evaluation of wheat yield in North China Plain under extreme climate by coupling crop model with machine learning. Comput. Electron. Agric. 217.

Boken, V.K., 2000. Forecasting spring wheat yield using time series analysis: a case study for the Canadian Prairies. Agron. J. 92 (6), 1047–1053.

Chen, X.G., Li, Y., Yao, N., Liu, D.L., Javed, T., Liu, C.C., Liu, F.G., 2020. Impacts of multi-timescale SPEI and SMDI variations on winter wheat yields. Agric. Syst. 185, 14.

Chiru Naik, D., Chavan, S.R., Sonali, P., 2023. Incorporating the climate oscillations in the computation of meteorological drought over India. Nat. Hazards 117 (3), 2617–2646.

Dai, A.G., 2011. Characteristics and trends in various forms of the Palmer Drought Severity Index during 1900–2008. J. Geophys. Res. Atmos. 116, 26.

Dar, E.A., Brar, A.S., Dar, S.A., Aljuaid, B.S., El-Shehawi, A.M., Rashid, R., Shah, Z.A., Yousuf, A., Bhat, M.A., Ahmed, M., et al., 2021. Quantitative response of wheat to sowing dates and irrigation regimes using CERES-Wheat model. Saudi J. Biol. Sci. 28, 6198–6208.

Ding, Z.L., Ali, E.F., Elmahdy, A.M., Ragab, K.E., Seleiman, M.F., Kheir, A.M.S., 2021. Modeling the combined impacts of deficit irrigation, rising temperature and compost application on wheat yield and water productivity. Agric. Water Manag. 244, 12.

Dixit, S., Jayakumar, K.V., 2022. A non-stationary and probabilistic approach for drought characterization using trivariate and pairwise copula construction (PCC) model. Water Resour. Manag. 36 (4), 1217–1236.

Dracup, J.A., Lee, K.S., Paulson, E.G., 1980. On the definition of droughts. Water Resour. Res. 16 (2), 297–302.

Duan, G., Niu, R., 2018. Lake area analysis using exponential smoothing model and long time-series landsat images in Wuhan, China. Sustainability 10 (2), 149. https://doi.org/10.3390/su10010149.

Duncan, L.L., Perrone, D., Jacobi, J.H., Hornberger, G.M., 2015. Drought planning and management: Using high spatial resolution as part of the solution. Environ. Sci. Technol. 49 (5), 2639–2647.

Geng, G., Yang, R., Liu, L., 2022. Downscaled solar-induced chlorophyll fluorescence has great potential for monitoring the response of vegetation to drought in the Yellow River Basin, China: Insights from an extreme event. Ecol. Indic. 138, 15.

Gunawat, A., Sharma, D., Sharma, A., Dubey, S.K., 2022. Assessment of climate change impact and potential adaptation measures on wheat yield using the DSSAT model in the semi-arid environment. Nat. Hazards 111, 2077–2096.

Hamed, K.H., Rao, A.R.A., 1998. A modified Mann-Kendall trend test for autocorrelated data. J. Hydrol. 204 (1), 182–196.

Han, W., Lin, X., Wang, D., 2023. Uncovering the primary drivers of regional variability in the impact of climate change on wheat yields in China. J. Clean. Prod. 421.

Hao, Z., AghaKouchak, A., 2013. Multivariate Standardized Drought Index: A parametric multi-index model. Adv. Water Resour. 57, 12–18.

He, J., Jones, J.W., Graham, W.D., Dukes, M.D., 2010. Influence of likelihood function choice for estimating crop model parameters using the generalized likelihood uncertainty estimation method. Agric. Syst. 103 (5), 256–264.

Huang, S., Chang, J., Leng, G., Huang, Q., 2015. Integrated index for drought assessment based on variable fuzzy set theory: A case study in the Yellow River basin, China. J. Hydrol. 527, 608–618.

Ishaque, W., Osman, R., Hafiza, B.S., Malghani, S., Zhao, B., Xu, M., Ata-Ul-Karim, S.T., 2023. Quantifying the impacts of climate change on wheat phenology, yield, and evapotranspiration under irrigated and rainfed conditions. Agric. Water Manag. 275.

Javed, T., Zhang, J.H., Bhattarai, N., Sha, Z., Rashid, S., Yun, B., Ahmad, S., Henchiri, M., Kamran, M., 2021. Drought characterization across agricultural regions of China using standardized precipitation and vegetation water supply indices. J. Clean. Prod. 313, 15.

Ji, Y., 2022. Frequency analysis of drought and its impact on water use efficiency of terrestrial ecosystems. Northwest Agriculture and Forestry University, Yangling. (In Chinese with English abstract).

Jones, J.W., Hoogenboom, G., Porter, C.H., Boote, K.J., Batchelor, W.D., Hunt, L.A., Wilkens, P.W., Singh, U., Gijsman, A.J., Ritchie, J.T., 2003. The DSSAT cropping system model. Eur. J. Agron. 18 (3–4), 235–265.

Kassie, B.T., Asseng, S., Porter, C.H., Royce, F.S., 2016. Performance of DSSAT-Nwheat across a wide range of current and future growing conditions. Eur. J. Agron. 81, 27–36.

Kumar, V., Chu, H.J., 2024. Seasonal drought severity identification using a modified multivariate index: A case study of Indo-Gangetic Plains in India. J. Hydrol. 629.

Leng, G., Hall, J., 2019. Crop yield sensitivity of global major agricultural countries to droughts and the projected changes in the future. Sci. Total. Environ. 654, 811–821.

Li, Q., Dong, B., Qiao, Y., Liu, M., Zhang, J., 2010a. Root growth, available soil water, and water-use efficiency of winter wheat under different irrigation regimes applied at different growth stages in North China. Agric. Water Manag. 97 (10), 1676–1682.

Li, B., Han, J., Gu, H., Yan, Z., Wang, L., Wang, B., Liu, X., 2026. Developing effective deep-rooted winter wheat cultivars improves adaptation to stored-soil-water irrigation in the North China Plain. Agric. Water Manag. 325.

Li, L., Peng, Q., Xu, J., Gu, X., Cai, H., 2024. Widespread enhancement and slower occurrence of agricultural drought events in drylands of the Yellow River Basin. J. Hydrol. Reg. Stud. 52.

Li, Y., Horton, R., Ren, T., Chen, C., 2010b. Prediction of annual reference evapotranspiration using climatic data. Agric. Water Manag. 97, 300–308.

Li, W.G., Liu, S.J., Hou, M.T., Han, J., Chen, X.M., 2021. Research progress of meteorological and agricultural drought index. Meteorol. Environ. Sci. 44 (03), 76–82.

Liu, J.C., Feng, H., He, J.Q., Chen, H.X., Ding, D.Y., Luo, X.Q., Dong, Q.G., 2019. Modeling wheat nutritional quality with a modified CERES-wheat model. Eur. J. Agron. 109, 9.

Liu, Y., Xue, W.L., 2022. Spatial and temporal evolution of agricultural drought and its characteristics of natural recovery period in the Yellow River Basin. Agric. Res. Arid. Areas 40 (02), 213–221.

Liu, Y., Chen, Q., Ge, J., Dai, J., 2018. Spatiotemporal variation of wheat phenology in China from 1981 to 2010 under the background of climate change. Sci. China Earth Sci. 48 (07), 888–898.

Liu, Z.X., Qiu, R.J., Zhang, Q., 2025. Differences in effects of varying compound extreme temperature and precipitation events on summer maize yield in North China. Agric. Water Manag. 307.

Long, X., Ju, H., Wang, J., Gong, S., Li, G., 2022. Impact of climate change on wheat yield and quality in the Yellow River Basin under RCP8.5 during 2020–2050. Adv. Clim. Change Res. 13 (3), 397–407.

Martinez-Fernandez, J., Gonzalez-Zamora, A., Sanchez, N., Gumuzzio, A., Herrero-Jimenez, C.M., 2016. Satellite soil moisture for agricultural drought monitoring: Assessment of the SMOS derived Soil Water Deficit Index (vol. 177, p. 277, 2016). Remote. Sens. Environ. 183, 368, 368.

McKee, T.B., Doesken, N.J., Kleist, J., 1993. The relationship of drought frequency and duration to time scales. Proceedings of the 8th Conference on Applied Climatology. American Meteorological Society, Boston, MA, pp. 179–183.

Mishra, A.K., Singh, V.P., 2010. A review of drought concepts. J. Hydrol. 391 (1–2), 202–216.

Moreno-Cadena, L.P., Hoogenboom, G., Fisher, M.J., Ramirez-Villegas, J., Prager, S.D., Becerra Lopez-Lavalle, L.A., Pypers, P., Mejia de Tafur, M.S., Wallach, D., Muñoz-Carpena, R., Asseng, S., 2020. Importance of genetic parameters and uncertainty of MANIHOT, a new mechanistic cassava simulation model. Eur. J. Agron. 115.

Mpelasoka, F., Hennessy, K., Jones, R., Bates, B., 2008. Comparison of suitable drought indices for climate change impacts assessment over Australia towards resource management. Int. J. Climatol. 28 (10), 1283–1292.

Ng, C.Y., Jaafar, W.Z.W., Othman, F., Lai, S., Mei, Y., Juneng, L., 2024. Assessment of Evaporative Demand Drought Index for drought analysis in Peninsular Malaysia. Sci. Total. Environ. 917.

Niu, B., Li, Y., De, L., Xie, L., Wang, L., Jiang, X., Feng, H., Yu, Q., He, J., Lin, H., 2024. Improved identification and monitoring of meteorological, agricultural, and hydrological droughts using the modified nonstationary drought indices in the Yellow River Basin of China. J. Hydrol. 643.

Palmer, W.C., 1965. Meteorological Drought. U.S. Department of Commerce, Weather Bureau, Washington, DC, p. 58.

Potop, V., Mozny, M., Soukup, J., 2012. Drought evolution at various time scales in the lowland regions and their impact on vegetable crops in the Czech Republic. Agric. For. Meteorol. 156, 121–133.

Rahimi-Moghaddam, S., Deihimfard, R., Azizi, K., Roostaei, M., 2021. Characterizing spatial and temporal trends in drought patterns of rainfed wheat (Triticum aestivum L.) across various climatic conditions: A modelling approach. Eur. J. Agron. 129, 16.

Rajagopalan, B., Lall, U., Tarboton, D.G., 1997. Evaluation of kernel density estimation methods for daily precipitation resampling. Stoch. Hydrol. Hydraul. 11 (6), 523–547.

Rashid, M.M., Beecham, S., 2019. Development of a non-stationary Standardized Precipitation Index and its application to a South Australian climate. Sci. Total. Environ. 657, 882–892.

Sadri, S., Wood, E.F., Pan, M., 2018. Developing a drought-monitoring index for the contiguous US using SMAP. Hydrol. Earth Syst. Sci. 22 (12), 6611–6626.

Sen, P.K., 1968. Estimates of the regression coefficient based on Kendall's tau. J. Am. Stat. Assoc. 63 (324), 1379–1389.

Shi, X., Chen, J., Ding, H., Yang, Y., Zhang, Y., 2024. Winter wheat yield estimation based on Sparrow Search Algorithm combined with Random Forest: A case study in Henan Province, China. Chin. Geogr. Sci. 34 (2), 342–356.

Shyrokaya, A., Messori, G., Pechlivanidis, I., Pappenberger, F., Cloke, H.L., Di Baldassarre, G., 2024. Significant relationships between drought indicators and impacts for the 2018–2019 drought in Germany. Environ. Res. Lett. 19 (1).

Silverman, B.W., 1986. Density Estimation for Statistics and Data Analysis. Chapman and Hall, New York.

Sun, S., Yang, X.G., Zhang, Z.T., Zhao, J., Liu, Z.J., 2021. Effects of different levels of drought on winter wheat yield in North China Plain. Chin. J. Agric. Eng. 37 (14), 69–78.

Tao, F., Zhang, L., Zhang, Z., Chen, Y., 2022. Climate warming outweighed agricultural managements in affecting wheat phenology across China during 1981–2018. Agric. For. Meteorol. 316.

Torrence, C., Compo, G.P., 1998. A practical guide to wavelet analysis. Bull. Am. Meteorol. Soc. 79 (1), 61–78.

Trnka, M., Brazdil, R., Mozny, M., Stepanek, P., Dobrovolny, P., Zahradnicek, P., Balek, J., Semeradova, D., Dubrovsky, M., Hlavinka, P., Eitzinger, J., Wardlow, B., Svoboda, M., Hayesi, M., Zalud, Z., 2015. Soil moisture trends in the Czech Republic between 1961 and 2012. Int. J. Climatol. 35 (13), 3733–3747.

Vicente-Serrano, S.M., Begueria, S., Lopez-Moreno, J.I., 2010. A multiscalar drought index sensitive to global warming: The Standardized Precipitation Evapotranspiration Index. J. Clim. 23 (7), 1696–1718.

Vidal, J.P., Martin, E., Franchistéguy, L., Habets, F., Soubeyroux, J.M., Blanchard, M., Baillon, M., 2010. Multilevel and multiscale drought reanalysis over France with the

Safran-Isba-Modcou hydrometeorological suite. Hydrol. Earth Syst. Sci. 14 (3), 459–478.
Wang, W., Yang, H., Huang, S., Wang, Z., Liang, Q., Chen, S., 2024. Trivariate copula functions for constructing a comprehensive atmosphere-land surface-hydrology drought index: A case study in the Yellow River basin. J. Hydrol. 642.
Wang, X., Luo, P., Zheng, Y., Duan, W., Wang, S., Zhu, W., Zhang, Y., Nover, D., 2023a. Drought disasters in China from 1991 to 2018: Analysis of spatiotemporal trends and characteristics. Remote. Sens. 15 (6).
Wang, Y., Wang, S., Zhao, W., Liu, Y., 2022. The increasing contribution of potential evapotranspiration to severe droughts in the Yellow River basin. J. Hydrol. 605.
Wang, Y., Wang, S., Chen, Y., Wang, F., Liu, Y., Zhao, W., 2023c. Anthropogenic drought in the Yellow River basin: Multifaceted and weakening connections between meteorological and hydrological droughts. J. Hydrol. 619.
Wang, Y., Peng, T., He, Y., Singh, V.P., Lin, Q., Dong, X., Fan, T., Liu, J., Guo, J., Wang, G., 2023b. Attribution analysis of non-stationary hydrological drought using the GAMLSS framework and an improved SWAT model. J. Hydrol. 627.
Wei, Y., Ru, H., Leng, X., He, Z., Ayantobo, O.O., Javed, T., Yao, N., 2022. Better performance of the modified CERES-Wheat model in simulating evapotranspiration and wheat growth under water stress conditions. Agric. -Basel 12 (11).
Wei, Y., Zhang, Z., Hou, M., Zhuo, L., Yao, N., Li, L., Xiangli, J., Javed, T., He, J., Yu, Q., 2025. Strategies for mitigating winter wheat yield reduction in the Yellow River basin: Simulations and insights from CMIP6 data and the improved DSSAT-CERES-wheat model. Agric. Water Manag. 318.
Wen, Q., Sun, P., Zhang, Q., Yao, R., 2020. Construction of nonstationary standardized precipitation evapotranspiration index and spatiotemporal pattern of future drought in China. Acta Geogr. Sin. 75 (07), 1465–1482.
Weng, B., Zhang, P., Li, S., 2015. Drought risk assessment in China with different spatial scales. Arab. J. Geosci. 8 (12), 10193–10202.
Wu, D., Yan, D., Yang, G., Wang, X., Xiao, W., Zhang, H., 2013. Assessment on agricultural drought vulnerability in the Yellow River basin based on a fuzzy clustering iterative model. Nat. Hazards 67 (2), 919–936.
Wu, J., Chen, X., 2019. Spatiotemporal trends of dryness/wetness duration and severity: The respective contribution of precipitation and temperature. Atmos. Res. 216, 176–185.
Wu, J., Chen, X., Yao, H., Gao, L., Chen, Y., Liu, M., 2017. Non-linear relationship of hydrological drought responding to meteorological drought and impact of a large reservoir. J. Hydrol. 551, 495–507.
Wu, J., Wang, N., Shen, H., Ma, X., 2022. Spatial–temporal variation of climate and its impact on winter wheat production in Guanzhong Plain. China Comput. Electron. Agric. 195.
Xu, X., Su, P., Jiang, X., Ye, X., Zeng, Y., 2020. Effects of climate warming on growth, yield and quality of winter wheat. Chin. Agric. Sci. Bull. 36 (25), 101–105.
Yang, Y., Wang, W., Zhang, H., Liao, L., Wang, T., Yang, J., Xie, X., Li, X., 2024. The quantitative inhibition effects of meteorological drought on sugarcane growth using the Decision Support System for Agrotechnology Transfer-CANEGRO model in Laibin, China. Agric. -Basel 14 (3).
Yao, N., Song, L., Liu, J., Feng, H., Wu, S., He, J., 2015c. Effects of water stress at different growth stages on growth, development and yield of winter wheat in arid regions. Sci. Agric. Sin. 48 (12), 2379–2389.
Yao, N., Li, Y., Xu, F., Liu, J., Chen, S., Ma, H.J., Chau, H.W., Liu, D., Li, M., Feng, H., Yu, Q., He, J.Q., 2020b. Permanent wilting point plays an important role in simulating winter wheat growth under water deficit conditions. Agric. Water Manag. 229, 15.
Yao, N., Li, L., Feng, P., Feng, H., Liu, D.L., Liu, Y., Jiang, K., Hu, X., Li, Y., 2020a. Projections of drought characteristics in China based on a standardized precipitation and evapotranspiration index and multiple GCMs. Sci. Total. Environ. 704, 18.
Yao, N., Li, Y., Liu, Q., Zhang, S., Chen, X., Ji, Y., Liu, F., Pulatov, A., Feng, P., 2022. Response of wheat and maize growth-yields to meteorological and agricultural droughts based on standardized precipitation evapotranspiration indexes and soil moisture deficit indexes. Agric. Water Manag. 266.
Yao, N., Wei, Y., Jiang, K., Liu, J., Li, Y., Ran, H., Javed, T., Feng, H., Yu, Q., He, Q., 2025. Nonlinear water stress response functions can improve the performance of the DSSAT-CERES-Wheat model under water deficit conditions. Agric. Water Manag. 307.
Zhang, D., Wang, H., Li, D., Li, H., Ju, H., Li, R., Batchelor, W., Li, Y., 2019. DSSAT-CERES-Wheat model to optimize plant density and nitrogen best management practices. Nutr. Cycl. Agroecosyst. 114, 19–32.
Zhang, X., Qin, W., Chen, S., Shao, L., Sun, H., 2017. Responses of yield and WUE of winter wheat to water stress during the past three decades: A case study in the North China Plain. Agric. Water Manag. 179, 47–54.
Zhao, X., Xia, H., Pan, L., Song, H., Niu, W., Wang, R., Li, R., Bian, X., Guo, Y., Qin, Y., 2021. Drought monitoring over Yellow River Basin from 2003 to 2019 using reconstructed MODIS land surface temperature in Google Earth Engine. Remote. Sens. 13 (18), 23.
Zhou, K., Wang, Y., Chang, J., Zhou, S., Guo, A., 2021. Spatial and temporal evolution of drought characteristics across the Yellow River basin. Ecol. Indic. 131.